



*Supplement of*

## **The effect of ash, water vapor, and heterogeneous chemistry on the evolution of a Pinatubo-size volcanic cloud**

**Mohamed Abdelkader et al.**

*Correspondence to:* Mohamed Abdelkader (mohamed.ahmed@kaust.edu.sa)

The copyright of individual parts of the supplement might differ from the article licence.

## 1 Implementation of injection

We use the EMAC import and offemis submodels to initialize the SO<sub>2</sub>, water vapor, and volcanic ash. The emission rate is provided to the model via a prepared file that contains a four-dimensional field in space and time based on the model grid. The grid cells that correspond to the injection location are filled with the required emission rate, and the other cells are kept  
5 with zero values. For instance, for the 1s1-20km experiment, the grid cell that corresponds to the location of Pinatubo at 20km altitude is filled with the daily emission rate for SO<sub>2</sub>. We use the same file to initialize water vapor and volcanic ash. We use different emission rates for water vapor and volcanic ash. Then, the file is read by import submodel, and the tracers are associated with offemiss submodel.

10 Figure S1 shows the sulfur mass content in the atmosphere, accumulated deposited sulfur mass, and their sum we below refer as a net sulfur mass. The net sulfur mass was initially 8.5Mt for 17 Mt injection of SO<sub>2</sub>. However, by the end of 1993, the net sulfur mass decreases to 8Mt, which means the model lost only 5.8% of mass to numerical errors in two and half years of simulations. This model quality is essential to accurately calculate the aerosol, and especially ash, mass balance.

15 Figure S2b,c shows that the SAOD response to the water vapor mass and aging of volcanic ash. The increase of SAOD due to injection of water vapor is small compared to the increase due to injection of volcanic ash. In the va1 experiment, the SAOD increases (compared to 1s1) by 0.14 independent of the amount of injected water vapor. Although in va0, the sulfate mass increases by 5.5Mt (Fig. S2c), the rise in SAOD is lower than in the case with aging volcanic ash (Fig. S2d). The effect of ash is seen for about two months, and then the SAOD relaxes to that we see in the 1s1 simulation. The sensitivity to the  
20 water vapor is low because the oxidation rate of SO<sub>2</sub> depends on the water remaining in volcanic cloud, which is limited by the temperature at the injection height. It happens that in the experiments with an injection of 15Mt and 150 Mt of water vapor at 20km, about the same amount of extra water retains in the stratosphere (Fig. S2e-j). In case of 150Mt injection at 25km, about 70Mt of water vapor is retained above 50hPa level(Fig. S2e,g,i). In the va1-20km experiment only 20Mt of extra water vapor is retained above 50hPa. The difference in water vapor mass in these experiments (20Mt compared to 70Mt) resulted from the  
25 different immersion freezing at the injection level defined by the ambient temperature. The remaining water vapor mass in all cases affects the formation rate of SO<sub>4</sub><sup>2-</sup> and the associated aerosol (Fig. S2).

Figure S3a shows the hovmoller diagram of SO<sub>4</sub><sup>2-</sup> accumulated removal mass by sedimentation, scavenging, and turbulent deposition in the va1-20km experiment. Sulfate aerosols are removed mostly in Intertropical Convergence Zone (ITCZ)  
30 and in the storm tracks, in agreement with ?. Fig. S3b shows the global accumulated sulfur deposition mass in different experiments. The sulfate removal in the 1s1 experiment is significantly lower than in other cases. Injection of water vapor increases the total removal of sulfate in the 1w1 experiment mainly because of larger sulfate mass (see Fig. 11 in the main text). In the va0 experiment, deposition increases due to the enhanced production of sulfate in the presence of ash particles. The aging of volcanic ash increases sulfate removal because aged particles are bigger and have larger deposition velocity. Also, in this

35 experiment, sulfate mass grows faster because the oxidation rate is enhanced by the heterogeneous reactions, which leads to  
the increase of the deposition mass.

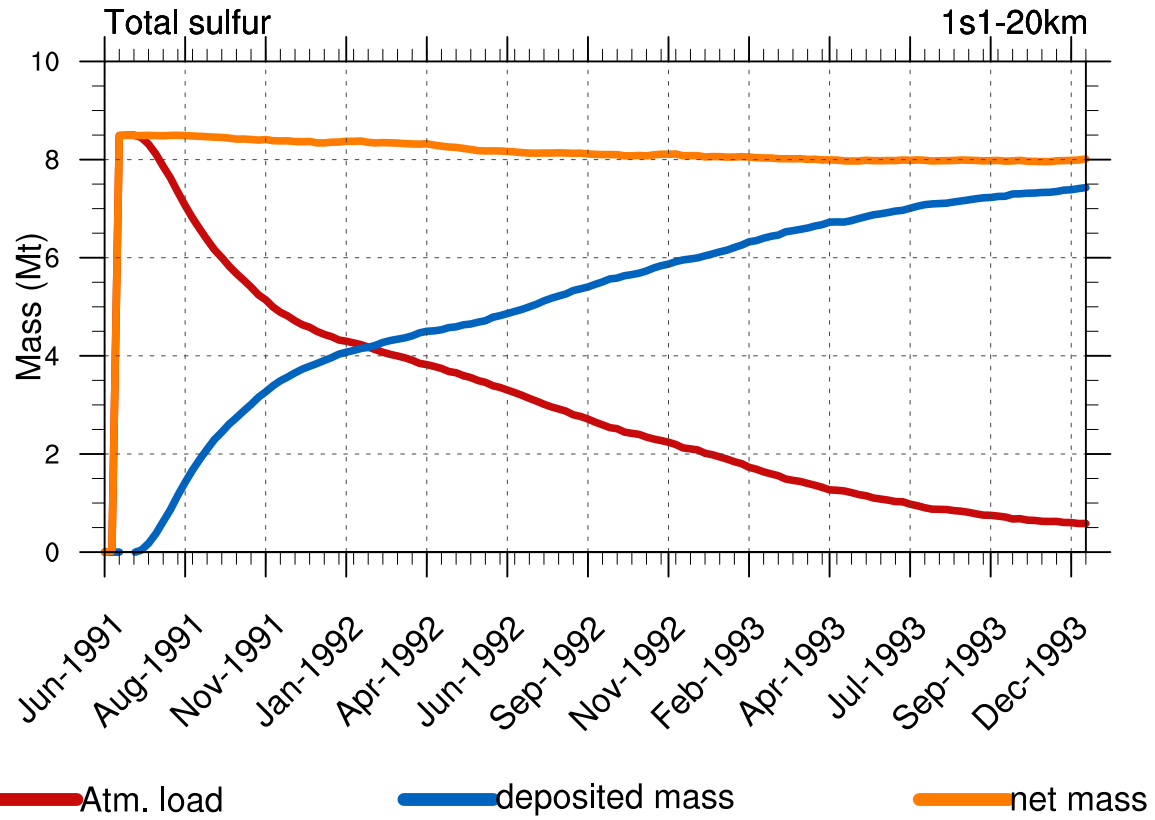
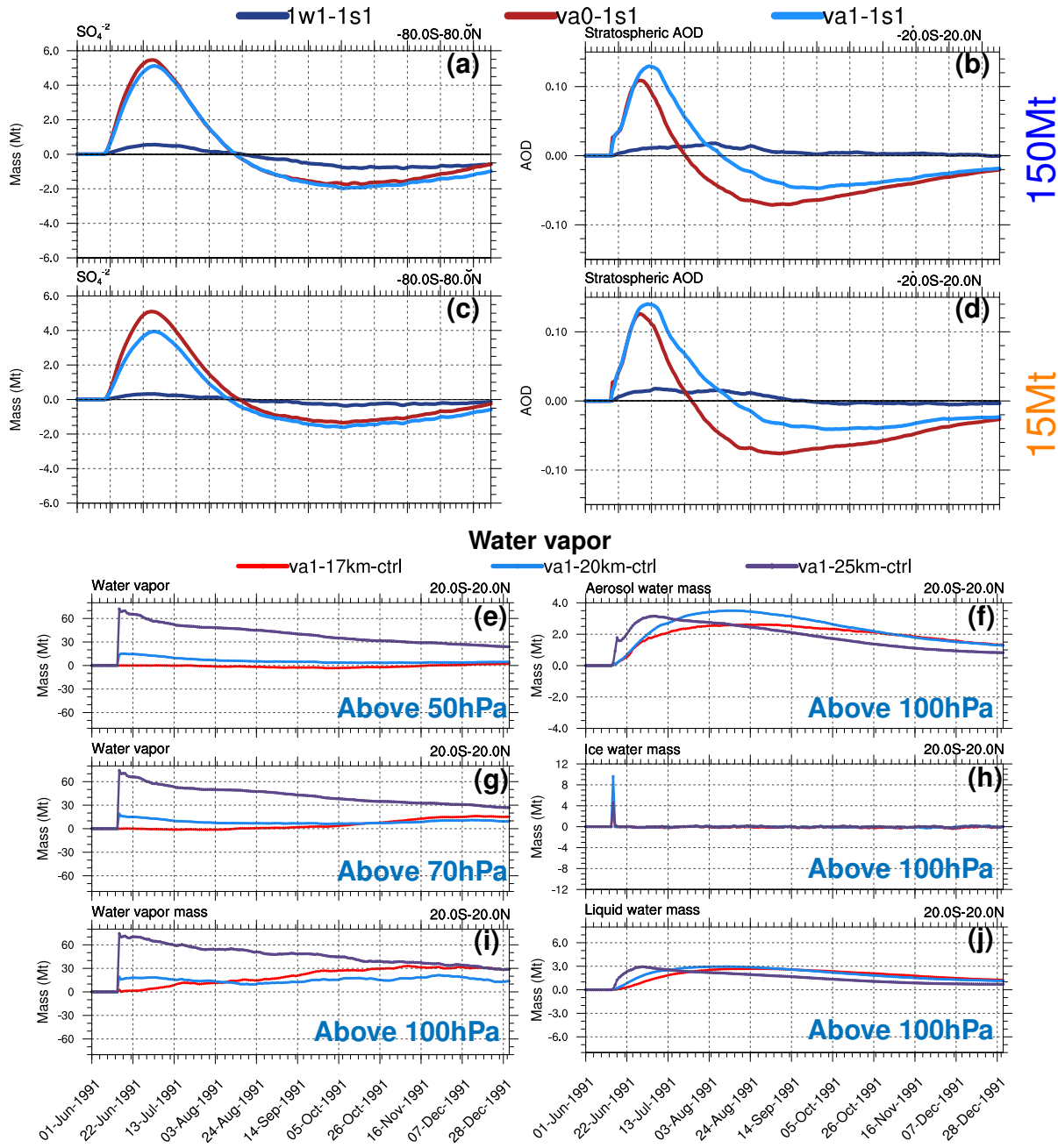


**Figure S1.** Time series for the total sulfur mass closure for 1s1-20km experiment *Atm. load* is the atmospheric sulfur mass, *Deposited mass* is the total deposition of sulfur, and *net mass* is the net atmospheric mass (Atmo. load+Deposited mass).

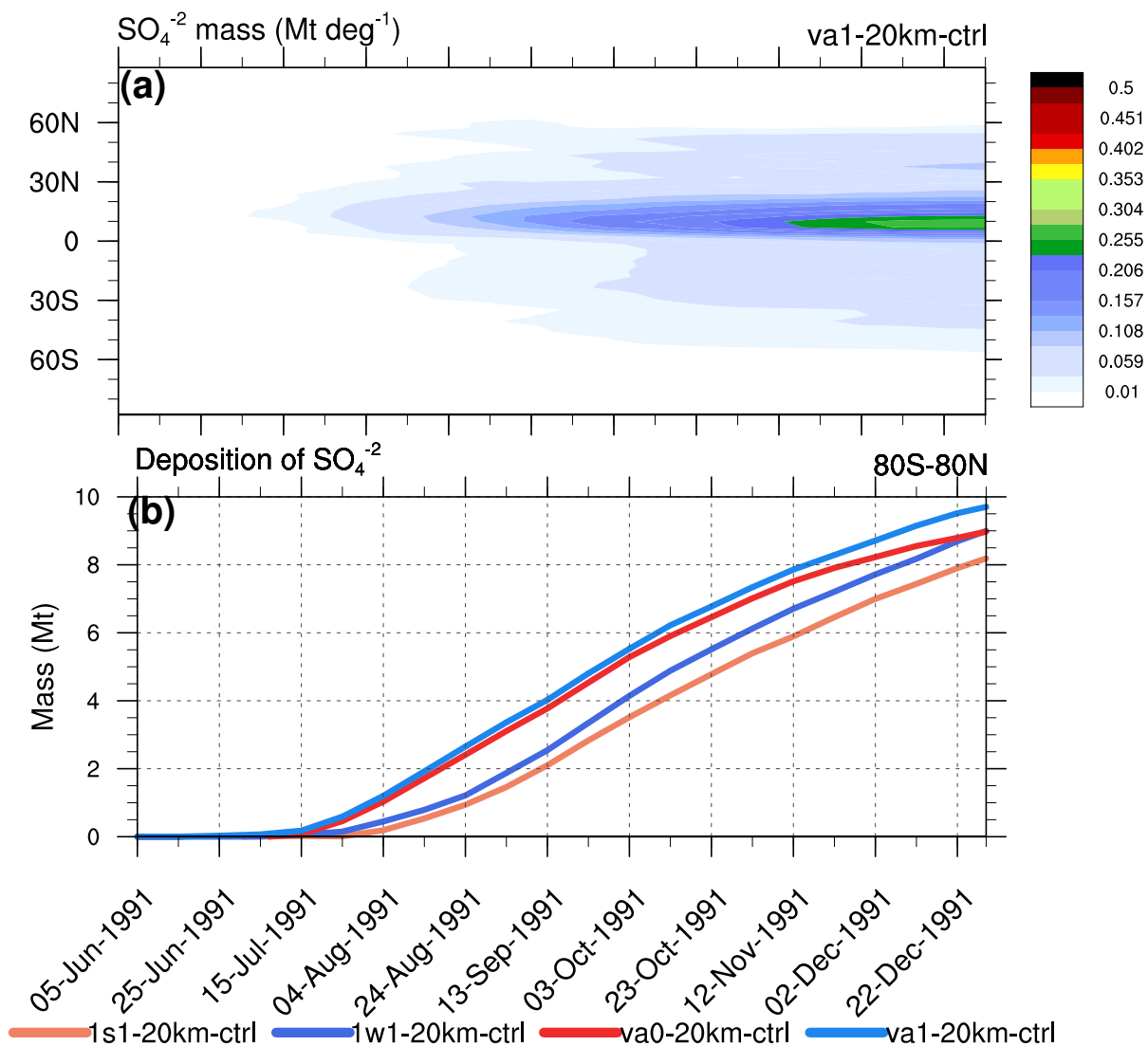
**Table S1.** Real and imaginary radiative indices for the volcanic ash as a function of wavelength

wave length ( $\mu\text{m}$ ).	real	imaginary
0.31	1.53	0.02
0.42	1.53	0.01
0.52	1.53	0.01
0.63	1.53	0.00
0.75	1.53	0.00
0.88	1.53	0.00
1.00	1.53	0.00
1.13	1.53	0.00
1.34	1.53	0.01
1.64	1.53	0.01
1.93	1.53	0.01
2.23	1.53	0.01
2.58	1.48	0.02
2.99	1.47	0.02

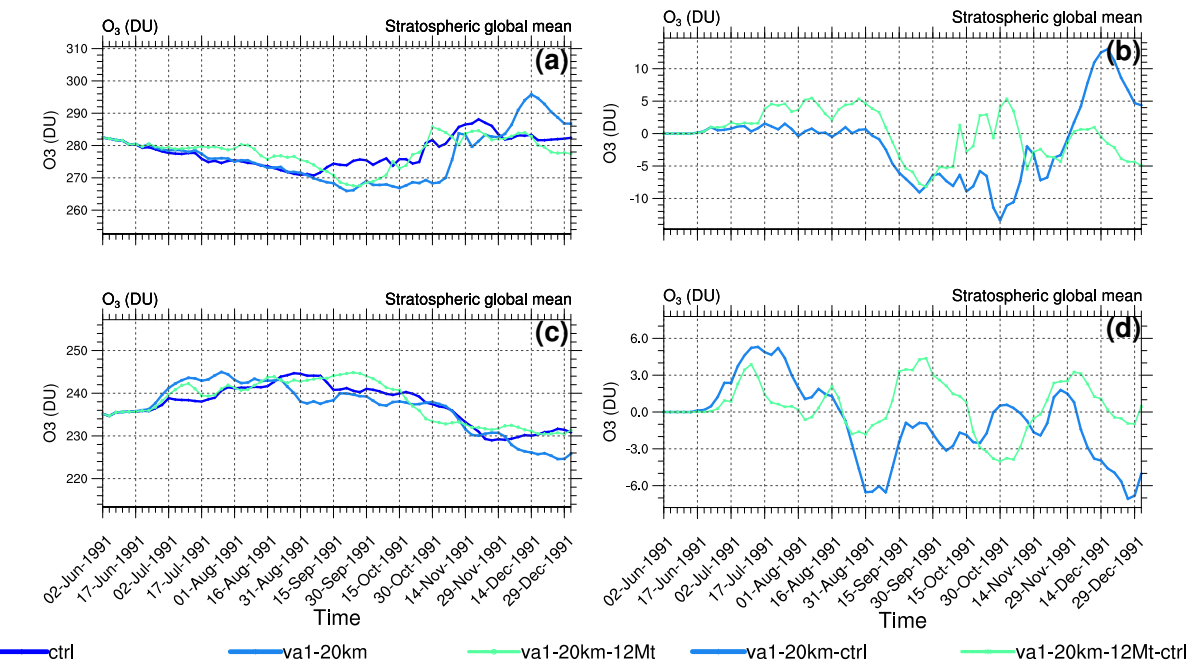
## Change in sulfate mass and AOD



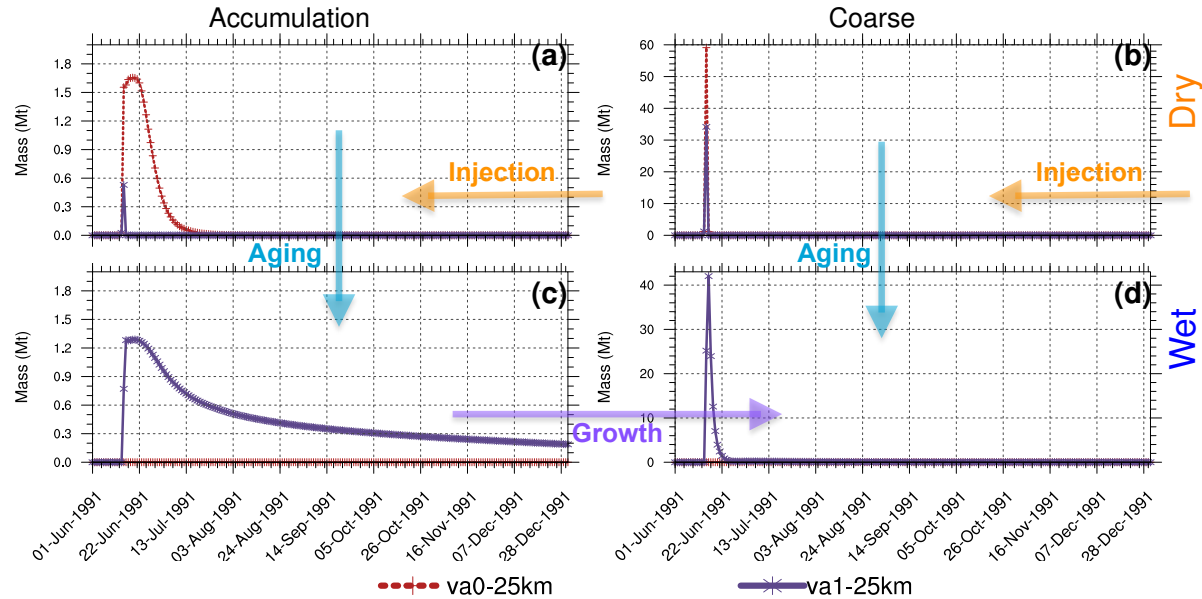
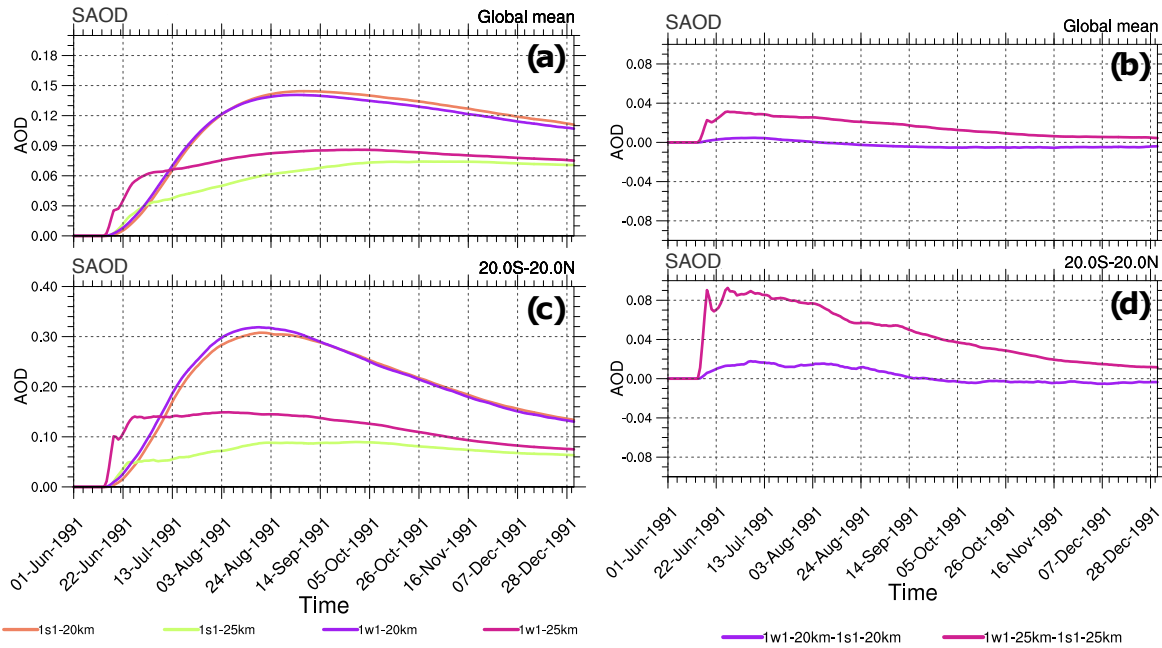
**Figure S2.** Upper four panels (a-d); Time series for the sensitivity of sulfate mass and equatorial SAOD to the amount of injected water vapor at 20km height in the presence of aged and non-aged volcanic ash: a) global sulfate mass for 150 Mt injected water vapor, b) SAOD for 150Mt injected water vapor, c) same as a using 15Mt water vapor, and d) same as b using 15 Mt water vapor. Lower six panels (e-j) time series for the change in the stratospheric water mass due to different injection heights for va1 experiment: e,g,i) stratospheric water vapor mass above 50 hPa, 70 hPa and 100 hPa respectively, f) aerosol water, g) ice, h) cloud liquid water above 100 hPa.



**Figure S3.** Total accumulated sulfate removal (scavenging + sedimentation) for va1-20km experiment; a) hovmöller diagram (total removal per unit degree of latitude), b) time series for the total integrated removal of  $\text{SO}_4^{2-}$  for different experiments.



**Figure S4.** Time series for stratospheric ozone in Dobson unit: a) the global mean, b) the change in the global mass w.r.t control simulation, c) equatorial mean (20S-20N), d) the change in equatorial mean w.r.t control simulation for the va1-20km and va1-20km-12Mt simulations.



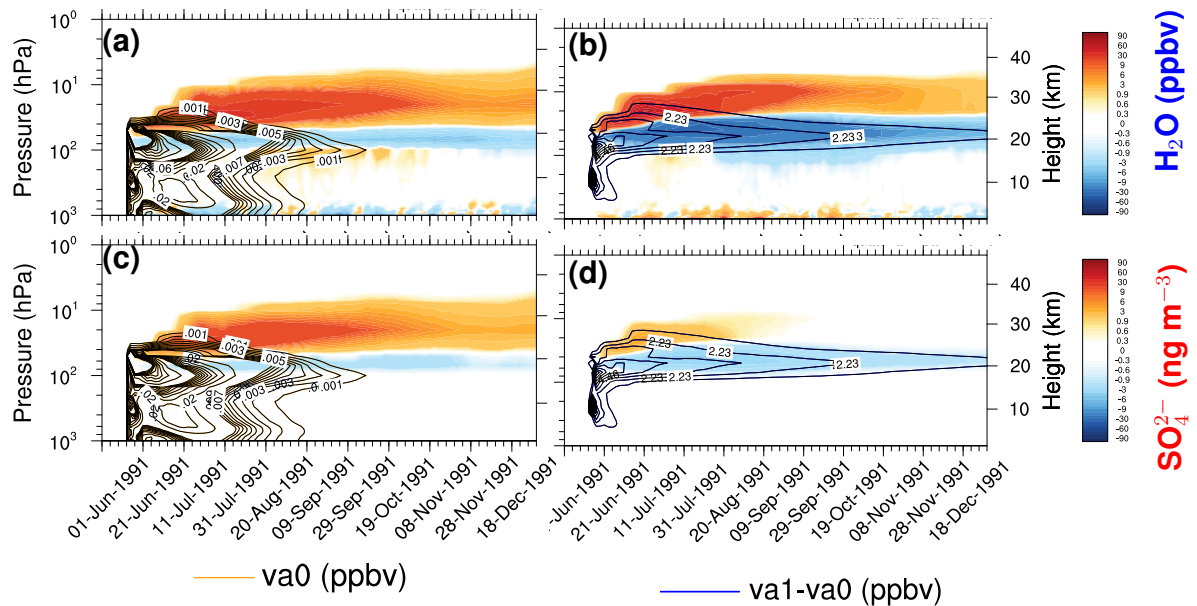


**Figure S7.** 20S-20N average perturbations of chemical constituents as function of pressure (from 300 hPa to 1 hPa) and time in va0-20km and va1-20km experiments. a)  $\text{H}_2\text{O}$  in va0-1w1 (ppbv), b)  $\text{H}_2\text{O}$  in va1-va0 (ppbv), c)  $\text{SO}_4^{2-}$  in va0-1w1 ( $\text{ngm}^{-3}$ ), d)  $\text{SO}_4^{2-}$  in va1-va0 ( $\text{ng m}^{-3}$ ). The contour lines shows the accumulation mode ash mixing ratio (ppbv); orange contour lines for va0 and blue contour lines for val-va0 in the (a-d) panels.

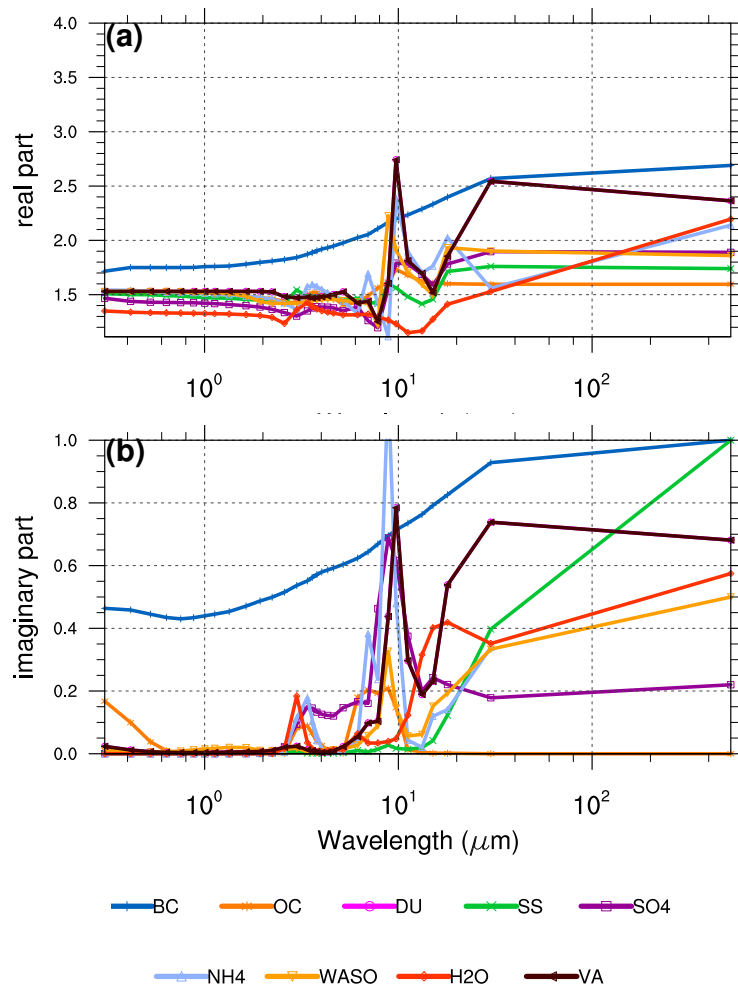


**Figure S8.** Radiative indices for different aerosols used in EMAC: a)real part, b) imaginary part.

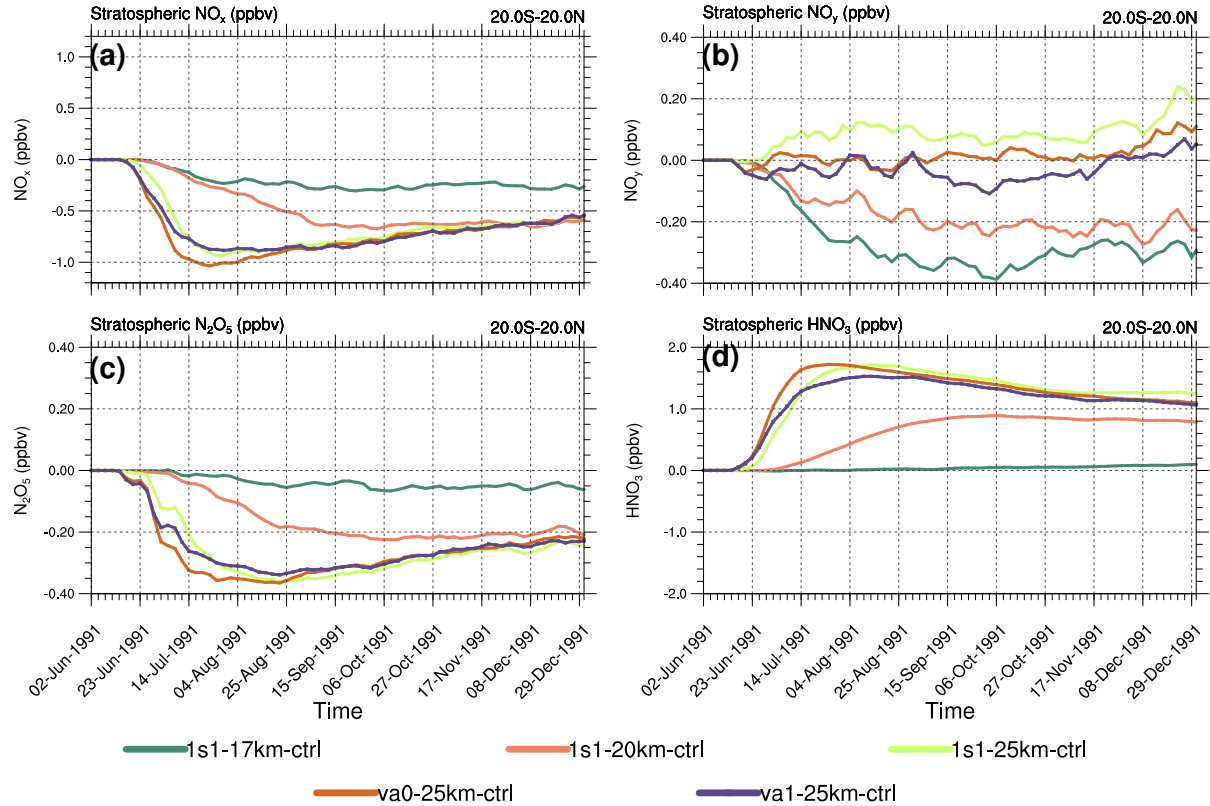


**Figure S9.** Time series for the stratospheric equatorial mixing ratio of: a)  $\text{NO}_x$ , b)  $\text{NO}_y$ , c)  $\text{N}_2\text{O}_5$ , d)  $\text{HNO}_3$ .

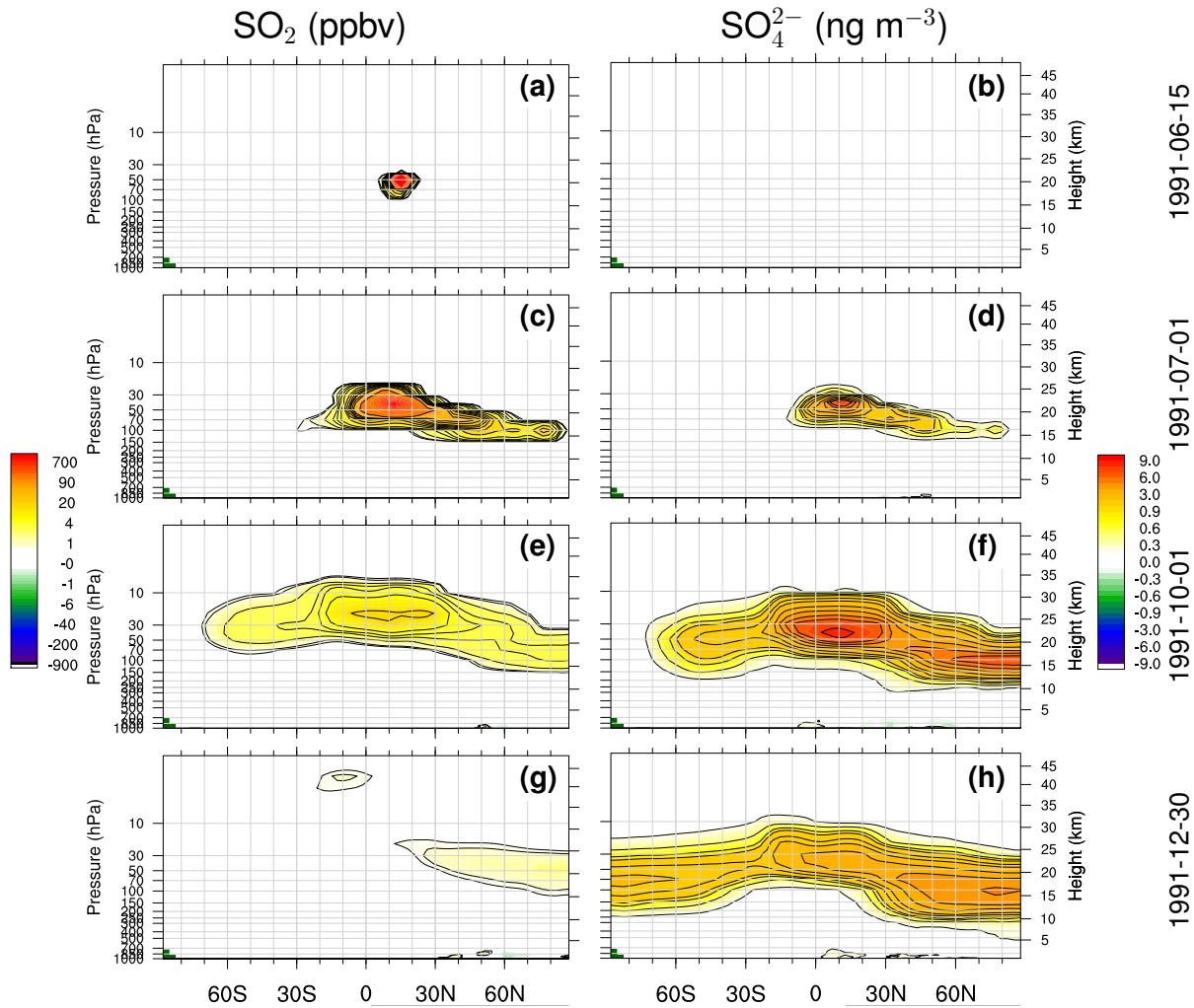


**Figure S10.** Zonal cross section for 1s1-20km experiment: a,c,e,g)  $\text{SO}_2$  (ppbv) and b,d,f,h)  $\text{SO}_4^{2-}$  ( $\text{ng m}^{-3}$ ) at selected times from top to bottom 15<sup>th</sup> June 1991, 1<sup>st</sup> July 1991, 1<sup>st</sup> October 1991, 30<sup>th</sup> December 1991.

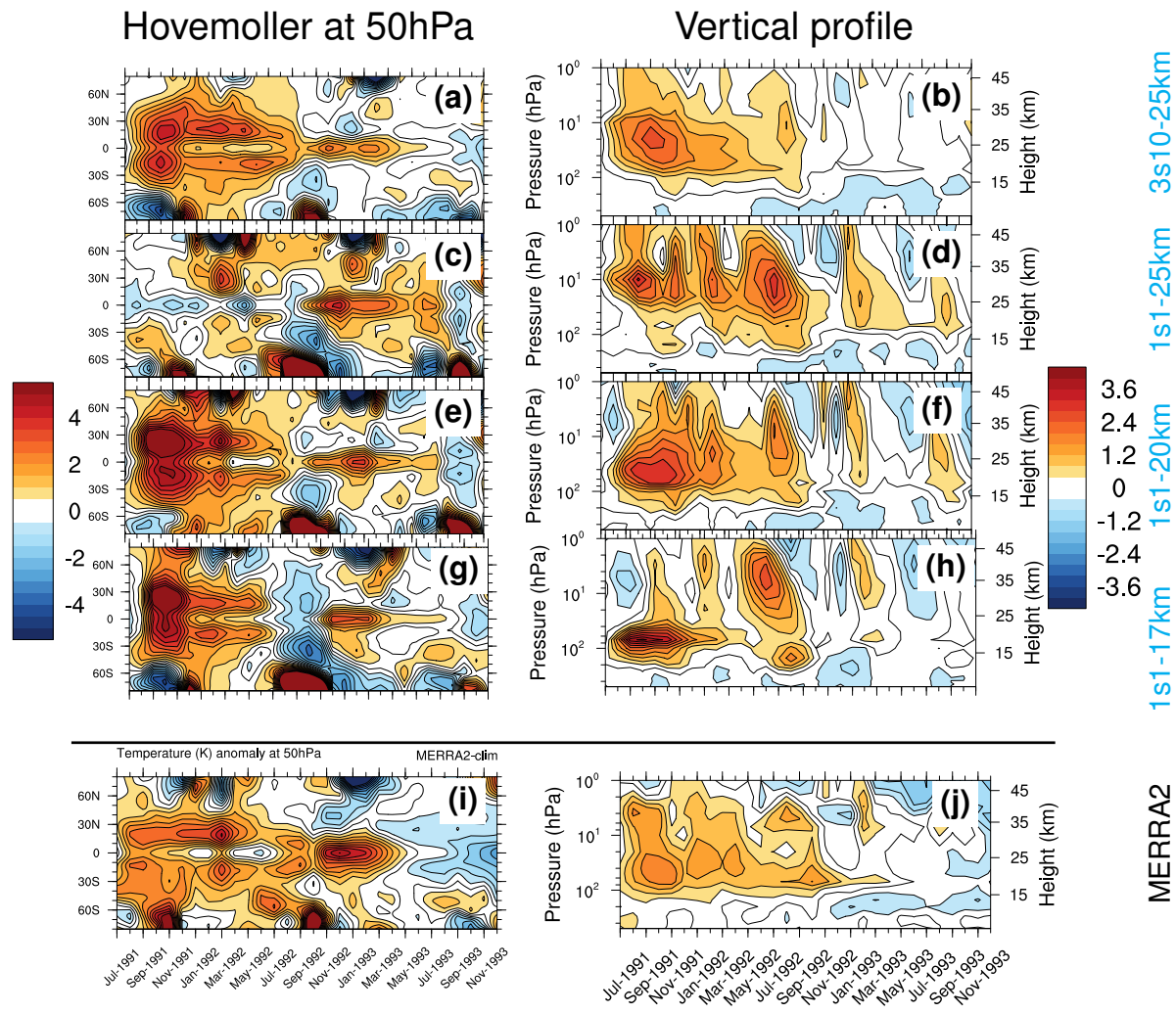


**Figure S11.** Atmospheric temperature anomalies (K) for the post-Pinatubo period with respect to the 1990-2000 climatology from the 3s10-25km (a,b), 1s1-25km (c,d), 1s1-20km (e,f), 1s1-17km (g,h), and MERRA-2 reanalysis (i,j). The left column depicts zonally average anomalies at the 50 hPa pressure level as a function of time and latitude, and the right column depicts globally (70S-70N) averaged anomalies as a function of time and height/pressure.